Mitigation of UWB radar self-motion for mm-Scale vibration detection

Xujun Ma, Pei Wang, Luan Chen, Fusang Zhang, Daqing Zhang

▶ **To cite this version:**

Xujun Ma, Pei Wang, Luan Chen, Fusang Zhang, Daqing Zhang. Mitigation of UWB radar self-motion for mm-Scale vibration detection. 2022 IEEE MTT-S International Wireless Symposium (IWS), Aug 2022, Harbin, China. pp.1-3, 10.1109/IWS55252.2022.9978061 . hal-04872831

HAL Id: hal-04872831
https://hal.science/hal-04872831v1

Submitted on 8 Jan 2025

HAL is a multi-disciplinary open access archive for the deposit and dissemination of scientific research documents, whether they are published or not. The documents may come from teaching and research institutions in France or abroad, or from public or private research centers.

L'archive ouverte pluridisciplinaire **HAL**, est destinée au dépôt et à la diffusion de documents scientifiques de niveau recherche, publiés ou non, émanant des établissements d'enseignement et de recherche français ou étrangers, des laboratoires publics ou privés.

Copyright

Mitigation of UWB Radar Self-Motion for mm-Scale Vibration Detection

Xujun Ma*, Pei Wang*, Luan Chen*, Fusang Zhang#, Daqing Zhang*
*Télécom SudParis, 91000 Évry, France
#Institute of Software, Chinese Academy of Sciences, Beijing 100190, China

***Abstract*—To reliably detect a target's mm-scale vibration with a handheld ultra-wideband (UWB) radar system, it is essential to mitigate radar self-motion (RSM) caused by unavoidable hand shaking. In this paper, to further mitigate the effect of stationary objects surrounding the target in real deployment environment, a more practical RSM signal model is proposed. Affected by adjacent objects and RSM, traditional variance-based target positioning method becomes unreliable and the quality of target signal degrades severely as the target's position is often estimated inaccurately. To tackle this problem, an extended bin selection strategy is adopted by considering multiple range bins around the target and independent component analysis (ICA) is leveraged to separate target motion and RSM. Experiments are conducted to verify the proposed technique, and a mm-scale mechanical vibration is reliably detected from 0.5-2m away with the handheld UWB radar system, achieving a median frequency estimation error rate lower than 3.7% under different adjacent environments.**

***Keywords*—Adjacent objects, handheld UWB radar, independent component analysis, radar self-motion (RSM).**

I. Introduction

With the recent advance in radar miniaturization, portable microwave radar system has been widely studied for short-range non-contact sensing applications, such as mechanical vibration detection [1], vital sign monitoring [2], and gesture recognition [3]. However, in most of the application scenarios, radar systems are required to be stationary instead of being held in user's hand, limiting the wide deployment of radar systems. To break this barrier and enable more handheld applications, several pilot studies have been conducted.

To track the large-scale RSM caused by operator's hand shaking and respiration motion, accelerometer-based [4] and accessory-radar-based techniques [5] are proposed, with which the RSM could be measured and cancelled at the cost of additional hardware. Alternatively, data-driven method using Empirical Mode Decomposition (EMD) [6] could also work by reconstructing target signal with Intrinsic Mode Functions (IMFs), however the performance highly depends on the frequency difference between RSM and target motion. Furthermore, a correlation-based method [7] is introduced to differentiate human target from background clutters which are then utilized to cancel the RSM in the received signal. In above studies, theoretical signal models are established by merely considering the vibrating target, whereas neglecting the influence of adjacent objects which commonly exist in real environments. Intuitively, due to adjacent objects and RSM, the received radar signal will be more complex and accurate target positioning may be more challenging. Thus, a more practical RSM signal model and corresponding detection methods are necessarily in need to enable the feasible retrieval of target's motion under RSM.

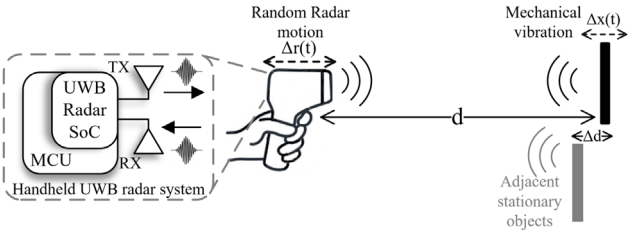

Fig. 1. Simplified block diagram of vibration detection using a handheld radar system containing the UWB radar frontend and processing unit. Mixed RF signals reflected from the vibrating target and adjacent objects are received by the UWB radar simultaneously.

In this paper, a new RSM mitigation method is proposed for mm-scale mechanical vibration detection in the presence of adjacent objects with handheld UWB radar. By considering adjacent stationary objects, a comprehensive signal model for handheld UWB radar is established and the side effect of adjacent objects on phase distortion and target positioning are discussed in detail. Instead of utilizing one fixed range bin for analysis, range bins are extended to cover both the target and its adjacent objects. Then, ICA is utilized to extract target motion from signals of all selected range bins. Extensive experiments are carried out to verify the effectiveness of the proposed method under different settings.

II. Analysis of UWB Radar Self-Motion

Fig. 1 shows the simplified block diagram of a vibration detection system using a handheld UWB radar. Assume the detection range is d, and the target vibration displacement is $\Delta x(t)$. The space between the target and adjacent objects is Δd. Due to RSM, the movement of UWB radar towards the target is depicted as $\Delta r(t)$.

Note that the UWB radar system on chip (SoC) transmits frequency-shifted Gaussian pulse periodically with a configurable pulse repetition frequency (PRF) f_p, and the carrier frequency is f_c=7.29 GHz. In the receiver (RX), right after the transmission of each pulse, the UWB radar utilizes direct RF sampling technique to digitalize the received signal, which provides the time-domain range profile for UWB radar. The reflected signal at RX can be expressed as:

$$R(t_n,\tau_m)=R_T(t_n,\tau_m)+R_S(t_n,\tau_m) \quad (1)$$

$$R_T(t_n,\tau_m)=V_T\, e^{\left[-\left(\tau_m-\tau_T(t_n)\right)^2/2\sigma^2\right]}\cos\left(2\pi f_c\left(\tau_m-\tau_T(t_n)\right)\right) \quad (2)$$

$$R_S(t_n,\tau_m)=\sqrt{\alpha}V_T e^{\left[-\left(\tau_m-\tau_S(t_n)\right)^2/2\sigma^2\right]}\cos\left(2\pi f_c\left(\tau_m-\tau_S(t_n)\right)\right) \quad (3)$$

where $\tau_T(t_n)=2[d+\Delta x(t_n)-\Delta r(t_n)]/c$ and $\tau_S(t_n)=2[d+\Delta d-\Delta r(t_n)]/c$ are the round-trip time delay from radar to the vibrating target and adjacent objects, respectively. $t_n=n/f_p$, $\tau_m=m/f_s$, n=1,2,…,N,

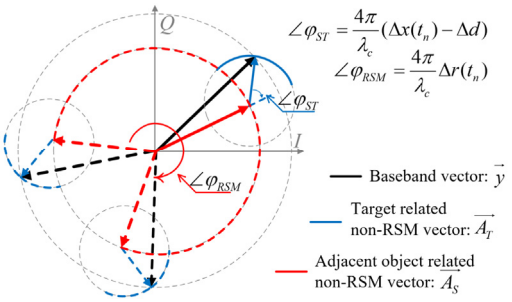

Fig. 2. Rotated of baseband and non-RSM vectors caused by RSM in the constellation plot.

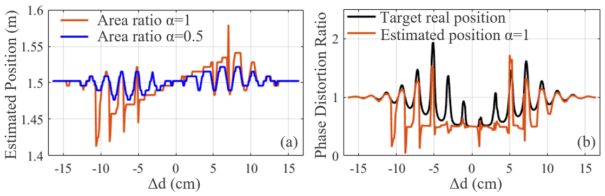

Fig. 3. Performance of variance-based target positioning under RSM. (a) Positioning results under different α and Δd. (b) Phase distortion comparison of signals extracted from real and estimated positions.

m=1,2,…,M, N represents the number of received frames, f_s is the sampling frequency and M stands for the number of samples of each frame. τ_m represents the sampling duration of each frame. $R_T(t_n,\tau_m)$ and $R_S(t_n,\tau_m)$ represent received pulses reflected on the target and adjacent objects, respectively. c is the speed of the light and σ determines the duration of the Gaussian pulse. V_T is the amplitude of the signal reflected from the target. Based on radar range equation, under the same detection range, the radar received signal power is proportional to radar cross section (RCS), which is highly related with target's physical size. Given that the target and its adjacent objects have the same RF reflectivity, the amplitude of $R_S(t_n,\tau_m)$ could be represented as $\sqrt{\alpha}V_T$, where α represents the area ratio between the target and its adjacent objects.

In the digital domain, by down-converting the received signal $R(t_n,\tau_m)$ with a complex carrier signal $\exp(j2\pi f_c\tau_m)$, the baseband signal could be retrieved as:

$$y(t_n,R_m)=\left[\underbrace{A_T(t_n,R_m)+A_S(t_n,R_m)}_{Non-RSM}\right]\underbrace{e^{-j\frac{4\pi}{\lambda_c}\Delta r(t_n)}}_{RSM} \quad (4)$$

$$A_T(t_n,R_m)=\frac{1}{2}V_T e^{\frac{-2(R_m-d+\Delta r(t_n)-\Delta x(t_n))^2}{c^2\sigma^2}} e^{j\frac{4\pi}{\lambda_c}(d+\Delta x(t_n))} \quad (5)$$

$$A_S(t_n,R_m)=\frac{1}{2}\sqrt{\alpha}V_T e^{\frac{-2(R_m-d+\Delta r(t_n)-\Delta d)^2}{c^2\sigma^2}} e^{j\frac{4\pi}{\lambda_c}(d+\Delta d)} \quad (6)$$

where λ_c is the wavelength of carrier frequency, $R_m=\tau_m\cdot c/2$ represents the range profile converted from the sampling duration τ_m. From Eq. (4)-(6), it can be seen that the baseband signal $y(t_n,R_m)$ could be decomposed into non-RSM and RSM vectors. For the non-RSM part, it consists of two vectors $A_T(t_n,R_m)$ and $A_S(t_n,R_m)$ whose phases contain target's motion and the constant delay of the adjacent objects, respectively. Whereas, for the RSM vector $e^{-j4\pi\Delta r(t_n)/\lambda_c}$, it contains RSM motion and accomplishes the rotation of non-RSM vectors. Fig. 2 demonstrates the rotation of the baseband vector $\vec{y}$

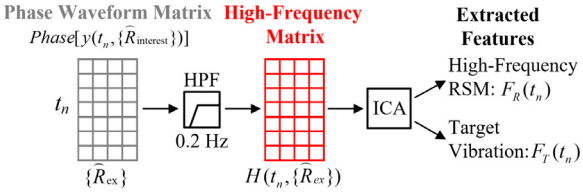

Fig. 4. Procedure of ICA-based RSM mitigation using signals from multiple range bins.

(black line) and two non-RSM vectors $\overrightarrow{A_T}$ (blue line) and $\overrightarrow{A_S}$ (red line) in the I/Q constellation plot. The angle difference φ_{ST} between $\overrightarrow{A_T}$ and $\overrightarrow{A_S}$ is mainly determined by Δd and Δx(t). Affected by the RSM, the superposed baseband vector would rotate around the origin. However, unlike an ideal arc, the rotation of the baseband vector is the non-linear combination of $\overrightarrow{A_T}$ and $\overrightarrow{A_S}$, thus causing phase distortion in $\vec{y}$.

III. Radar Self-Motion Mitigation Method

Normally, to locate the target position for stationary radar scenario, a variance-based searching method works well with the following function:

$$\hat{R}_{est}=\underset{R_m}{\text{argmax}}\left[var\left(y_{R_m}(t_n)\right)\right] \quad (7)$$

where $y_{R_m}(t_n)$ stands for the slow-time signal extracted from the m-th column in $y(t_n,R_m)$, and the range bin $\hat{R}_{est}$ with maximum variance is selected for target positioning. Regarding RSM scenario, to investigate whether the positioning performance of Eq. (7) will be affected by the adjacent stationary objects, simulations are first conducted with different Δd and α to quantify such impact. Specifically, by adjusting Δd from -16 to 16 cm while fixing target position d=1.5 m, the estimated range $\hat{R}_{est}$ under two area ratios (α=0.5 and 1) are shown in Fig. 3(a). Clearly, due to RSM, both two estimated $\hat{R}_{est}$ curves deviate from the target position, and the level of deviation enlarges as the area size of adjacent objects increases, leading to inaccurate estimation of target position.

To further depict the phase distortion of signals from the estimated position, phase distortion ratio is proposed by calculating the ratio between the target-related phase variation of the received signal and the theoretical phase variation, which is $4\pi\cdot\Delta x/\lambda_c$. Fig. 3(b) compares the phase distortion ratios of signals extracted from inaccurate positions (red line) against that from target's real position (black line) at 1.5 m. Clearly, phase distortion is inevitable even when signals are extracted from the correct position. However, the level of distortion could be even worse when inaccurate position is adopted. To properly handle this issue, an extended position searching method is proposed to cover the target position with the following function:

$$\{\hat{R}_{ex}\}=\underset{R_m}{\arg}\left[\frac{var\left(y_{\hat{R}_{est}}(t_n)\right)}{2}\le var\left(y_{R_m}(t_n)\right)\right] \quad (8)$$

where half of the maximum variance is set as the lower boundary for eligible range bins selection, forming a candidate set $\{\hat{R}_{ex}\}$. An ICA-based RSM mitigation method is proposed and illustrated in Fig. 4. Specifically, a high-pass filter with

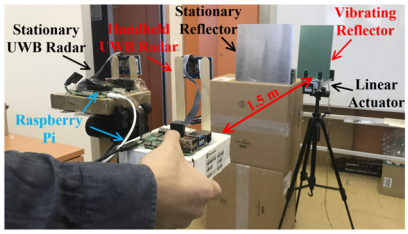

Fig. 5. Experimental setups for mechanical vibration detection using a handheld UWB radar. Another stationary UWB radar is utilized to provide ground truth.

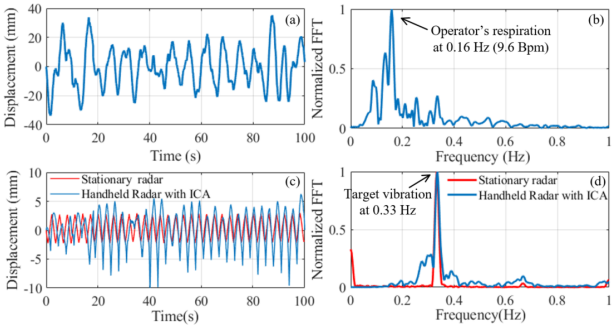

Fig. 6. (a) Waveform and (b) normalized FFT results of the first feature. (c) Waveform and (d) normalized FFT results of the second feature.

0.1 Hz stopband is first utilized to filter out low-frequency RSM from the phase waveform matrix formed by signals from $\{\hat{R}_{ex}\}$ and generate the high-frequency matrix $H(t_n, \{\hat{R}_{ex}\})$. After that, $H(t_n, \{\hat{R}_{ex}\})$ is taken as the input of ICA for statistical analysis to extract two dependent features, namely the high-frequency RSM $F_R(t_n)$ and target vibration $F_T(t_n)$.

IV. Experiments and Results

Experiments were carried out in the lab environment to verify the RSM mitigation technique. As shown in Fig. 5, two X4M05 UWB radar sensor modules [2] were configured by Raspberry Pi boards to work at 7.29 GHz with 50 Hz PRF and 23.328 GHz sampling rate. One UWB radar was held in hand while the stationary UWB radar was used to provide ground truth. Following the setup in Fig. 1, a 25 cm×15 cm metal reflector controlled by the linear actuator was located 1.5 m away from the handheld radar as target and a 30 cm×30 cm metal reflector was placed on the left side of the target as stationary object with an offset Δd=5 cm.

In the experiments, the linear actuator was programmed to move periodically at 0.33 Hz with 2.5 mm displacement. The handheld UWB radar was held for 100 s by a standing operator with normal body motion. After target position estimation using Eq. (8), the phase waveform matrix formed by range bins from 1.48-1.60 m was processed by the high-pass filter. Then, the generated higher-frequency component matrix was analysed by ICA to extract two independent features. As shown in Fig. 6(a) and Fig. 6(b), the first feature contains cm-scale periodical RSM signals mainly caused by operator's respiration motion at 0.16 Hz (9.6 bpm). In Fig. 6(c), the recovered mm-scale vibration waveform suffers from phase distortion as expected. Based on spectrum results in Fig. 6(d), the same spectrum peak at 0.33 Hz could be successfully detected by both the second feature and the stationary radar.

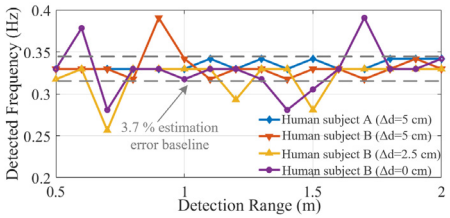

Fig. 7. Frequency measurement results of handheld radar detection conducted by two human subjects from 0.5-2 m with different Δd (5, 2.5, and 0 cm) setups. A median absolute deviation rate lower than 3.7% is achieved.

Furthermore, to evaluate the robustness of the proposed method, experiments were conducted by two human operators (subject A operated the radar more steadily than subject B) from 0.5 to 2 m with 0.1 m interval, and three Δd (5, 2.5, and 0 cm) were utilized to verify the detection performance under different levels of clutter. As shown in Fig. 7, detected frequency results match well with the ground truth frequency (0.33 Hz) for different ranges and Δd, and the median absolute frequency estimation error rate is lower than 3.7 %.

V. Conclusion

In this paper, a new RSM mitigation technique is proposed for mm-scale vibration detection with handheld UWB radar. To better analyse the impact of interferences near the target in real environment, a practical RSM signal model is introduced by considering adjacent objects. Affected by adjacent objects and RSM, phase distortion and positioning issues are addressed. To tackle these problems, strategies of multiple range bin selection and independent component analysis are utilized to extract target motion. Experimental results verify the robustness of the proposed technique for mm-scale mechanical vibration detection from different ranges with different operators and varied adjacent environments.

Acknowledgment

This work was supported in part by the EU CHIST-ERA RadioSense Project and the EU Horizon 2020 research and innovation programme IDEA-FAST (No. 853981).

References

[1] J. Wang et al., "Noncontact distance and amplitude-independent vibration measurement based on an extended DACM algorithm," *IEEE Trans. Instrum. Meas.*, vol. 63, no. 1, pp. 145–153, Jan. 2014.

[2] Andersen et al., "A 118-mW pulse-based radar SoC in 55-nm CMOS for non-contact human vital signs detection," *IEEE J. Solid-State Circuits*, vol. 52, no. 12, pp. 3421–3433, Dec. 2017.

[3] C. Gu, J. Wang, and J. Lien, "Motion sensing using radar: Gesture Interaction and Beyond," *IEEE Microwave Magazine*, vol. 20, no. 8, pp. 44-57, Aug. 2019.

[4] L. Ren et al., "High-amplitude motion cancellation method for handheld UWB Doppler radar," in Proc. *IEEE Top. Conf. BioWireleSS Technol.*, Jan. 2014, pp. 10–12.

[5] Y. Zhang et al., "An interference suppression technique for life detection using 5.75- and 35-GHz dual-frequency continuous-wave radar," *IEEE Geosci. Remote Sens. Lett.*, vol. 12, no. 3, pp. 482–486, Mar. 2015.

[6] I. Mostafanezhad et al., "Cancellation of unwanted Doppler radar sensor motion using empirical mode decomposition," *IEEE Sensors J.*, vol. 13, no. 5, pp. 1897–1904, May 2013.

[7] E. Cardillo, C. Li and A. Caddemi, "Vital sign detection and radar self-motion cancellation through clutter identification," *IEEE Trans. Microw. Theory Techn.*, vol. 69, no. 3, pp. 1932-1942, Mar. 2021.